

THE EFFECT OF INHOMOGENEITIES ON EVALUATION OF A FRACTAL DIMENSION FOR OBJECTS ON A LATTICE

G.R. HAMILTON, W.G. LAIDLAW* and R. MAIER

Department of Chemistry, University of Calgary, Calgary, Alberta, Canada T2N 1N4

R.B. FLEWELLING

East Kootenary College, Cranbrook, British Columbia, Canada

Received 21 July 1989

Abstract

A comparison of the covering properties of windows $m, m + 1$, where the window side l_m is $l_m = 2^m$, yields an expression for the fractal dimension D_m which displays directly effects due to periodicity and inhomogeneities. The structure of the D_m versus m curve gives insight into the nature of the representation of the fractal. In some cases bounds for D may be obtained and, if appropriate, the effect of the inhomogeneities due to boundaries, initial conditions, the pixel limit or periodicity can be removed.

1. Introduction

1.1. FRACTALS

Fractal dimension has been used to characterize properties of many objects of chemical and physical interest [1]: for example, the adsorption surface of catalysts can be assessed in terms of a fractal dimension; even the catalyst "reactivity" can be characterized with a fractal dimension [2]. In addition, a large number of physical processes (diffusion-limited aggregation [3] and invasion percolation [4,5] are but two examples) have a critical point c at which the object, for example the site density $A(L)$ descriptive of the process, takes on fractal properties. "Breakthrough" of a percolation process on a lattice is an example of such a critical point, and the critical parameter is p_c , the percolation threshold. In such cases, a density ρ_A^c , defined as the fraction of lattice sites occupied by the percolating fluid, scales with lattice size L according to a power law:

$$\rho_A^c \sim L^{D-d}, \quad (1)$$

where D is the fractal dimension (a "critical exponent") and d is the geometric or lattice dimension.

*To whom correspondence may be addressed.

The evaluation of the fractal dimension of a physical object, e.g. a catalyst surface, or of a physical process at a critical point can be obtained via eq. (1) using the density $\rho_A^c(L)$ measured for several different window sizes L . However, in many cases the "density" measurements are indirect and models of the objects or simulations of the process can provide additional insight. This is particularly the case when some understanding of the effect of boundaries, inhomogeneities, periodicity, etc. is potentially important.

Although some fractal objects can be analyzed by an algebraic model (cf. the Sierpinski Gasket [6(a)] or by the use of hyperscaling relations [7,8], the only way in which to obtain a detailed characterization of many fractals is by analyzing their lattice representation generated by an appropriate computer algorithm. For example, Wilkinson and Willemsen [5(b)] extracted values of critical exponents such as D from eq. (1) by plotting the value of $\rho_A^c(L)$ (averaged over many representations) versus the size L of the grid and equated the slope to $D - d$ (cf. fig. 1).

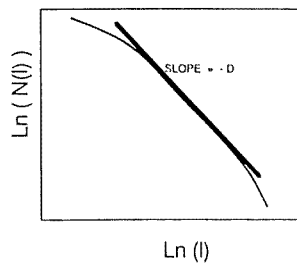


Fig. 1. Fractal dimension. From the number of objects of size l_m by l_m needed to cover the pattern versus the length l_m .

Generally one can, with the use of lattices, investigate directly a variety of effects simply by generating a representation of the fractal with the characteristics one wishes to study, be they boundaries, inhomogeneities, periodicity, etc. We shall in fact show that an analysis of the covering properties of windows with side l_m , where $l_m = 2^m$, $m, m + 1$, yields an expression for a fractal dimension D_m which displays directly effects due to periodicity and inhomogeneities. The structure of the D_m versus m curve then gives insight into the nature of the representation of the fractal. In some cases, bounds for D may be obtained and, if appropriate, the effect of the inhomogeneities due to boundaries, initial conditions, the pixel limit or periodicity can be removed.

1.2. MEASUREMENT OF D WITH ADJACENT WINDOWS l_m AND l_{m+1}

If one is near a critical point, the use of eq. (1) to extract D from a lattice representation requires a large number of realizations to reduce the scatter in ρ_A^c to acceptable levels and requires a range of L values. Alternatively, one may measure the

number of times $N(l_m)$ a window of size l_m must be laid down to cover all of a single lattice representation $A_c(L)$. The fractal dimension D is then the slope of:

$$\ln(N(l_m)) = -D \ln(l_m) + C. \tag{2}$$

This value of D , obtained in the limit as l_m goes to zero, has been denoted the "capacity dimension" D_c to distinguish it from the Hausdorff dimension [8]. Although, in principle, one needs only one grid size L , it must be large enough to permit a range of window sizes l_m , and in the best of circumstances yields a curve such as that depicted in fig. 1. Unfortunately, a plot of $N(l_m)$ using eq. (2) may not be the best tool for evaluating D . This is because eq. (2) is really a device for obtaining D by comparing $N(l_m)$ to that of $N(l = 1)$, i.e. for a window of size unity. To see this, note for $l_m = 1$, $C = \ln(N(l = 1))$, so that eq. (2) can be written as

$$D = \frac{\ln(N(l_m)/N(l = 1))}{\ln(1/l_m)}. \tag{3}$$

A more useful approach is to calculate D by comparing N for adjacent window sizes l_m and l_{m+1} as in

$$D_m = \frac{\ln(N(l_m)/N(l_{m+1}))}{\ln(l_{m+1}/l_m)}. \tag{4}$$

A plot of D_m versus m converts the curve of fig. 1 with its attractive "straight line" region into that of fig. 2. The more or less horizontal portion of this curve preserves the "straight line" portion of fig. 1, and a measure of D could be obtained by, say, averaging

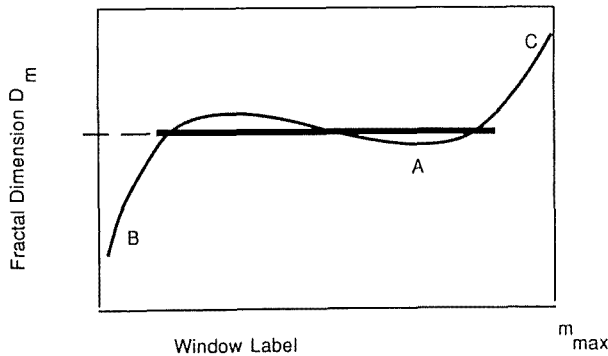


Fig. 2. Fractal dimension. Using eq. (4) with windows $m, m + 1$.

D over this region. However, one can, in fact, use the structure of this curve to advantage to obtain more insight into the fractal character of the object of interest.

1.3. CHARACTERISTICS OF REPRESENTATIONS ON A LATTICE

Physically defined fractal objects clearly have a lower limit, e.g. the atomic scale. Representations of fractal objects usually have lower limits where the dimension of a representation changes. In the case of a representation on a lattice, this will be referred to as the pixel limit [10] and is in fact usually the grid spacing. Fractals may also exhibit an upper limit which, in the case of lattice objects, is usually just the lattice extent [10], but if there is a "cut-off", this length may be less than the lattice extent L [6(b)]. In addition to these limiting factors, one can also consider the effect of boundary conditions on the object $A_c(L)$. An initial condition such as the arbitrary occupation of all lattice sites along part of the perimeter of the lattice (e.g. the source region of a percolation process) may create aberrations so that the fractal dimension appears to be different to that generated by the algorithm in the interior of the lattice. Similarly, the termination of the process may yield local inhomogeneities (e.g. near a sink). These situations may be influenced further by the conditions defining the boundaries, for example, closed boundaries may generate inhomogeneities, whereas the use of "periodic" boundaries normally reduced them. These features of a representation of a fractal on a lattice may all be viewed as the limitations on a presumed homogeneity, at all scales, of the representation. The problem then is one of inhomogeneities generated, on the lattice, by the restrictions on the algorithm.

2. Analysis

2.1. INHERENT INHOMOGENEITIES

In order to analyze in more detail the effect of inhomogeneities on a finite representation, consider the schematic of fig. 3(a), where a fractal object of dimension $D = 1.90$ spans an L by L grid. We now imagine that there is a large inhomogeneity A of dimension $D_A = 0.10$. Table 1 gives the number of windows $N(l_m)$ of size $l_m = (2)^m$ required to cover the occupied portions of the lattice. Using eq. (4), the dimension D_m given in the third column can be obtained. Since the intrusion has a dimension less than that of the object, its effect is to decrease the value of D_m when windows of size comparable to the inhomogeneity are employed in eq. (4). Consequently, there is a minimum in D_m near $m = 8$, i.e. at $l = 256$. Conversely, if the inhomogeneities were to have a larger value of D than the surrounding object, then for window sizes equal or less than that of the inhomogeneity, the measured value of D will simply be that of the inhomogeneity. This is the case for the limiting boundary $m = 9$ or at $l = 512$, where $D_m = 2.0$

To illustrate the effect of inhomogeneities comparable in size to the pixel, consider the situation illustrated by fig. 3(b), where the object has dimension $D = 2.00$ and the intrusions are of dimension zero and span a tree-like structure with branches of width 1, stem of width 2 and base of width 6. Table 1 again gives the $N(l_m)$ required and the D_m calculated using eq. (4). The inhomogeneity is now of lower dimension than

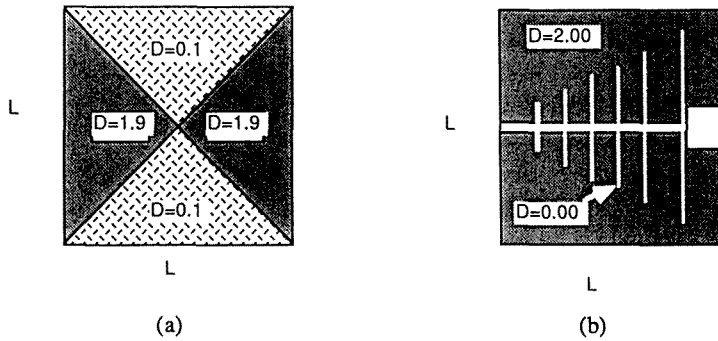


Fig. 3. (a) Effects of large-scale inhomogeneities. (b) Effects of pixel-scale inhomogeneities.

Table 1
Effects of inhomogeneities

(a) Large scale				(b) Small (pixel) scale			
$l_m = 2^m$	m	$N(l_m)$	D_m	$l_m = 2^m$	m	$N(l_m)$	D_m
512	9	0.98	} 2.00	128	7	1	} 2
256	8	3.93		64	6	4	
128	7	12.12	} 1.62	32	5	16	} 2
64	6	36.17		16	4	64	
32	5	118.30	} 1.71	8	3	256	} 2
16	4	413.14		4	2	1023	
8	3	1493.1	} 1.845	2	1	4040	} 1.998
4	2	5486.4		1	0	15728	
2	1	20321	} 1.878				} 1.981
1	0	75559					
			} 1.889				} 1.961
			} 1.950				
			} 1.897				

the object and lowers the calculated dimension when windows of size comparable to the inhomogeneity are used in eq. (4). Thus, for m about 4 or smaller, i.e. for $l < 16$, the value of D_m is pulled below its correct value.



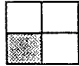



2.2. THE PIXEL LIMIT

The foregoing illustrations certainly show how an inhomogeneity in a fractal object can affect the measured value of D . Such inhomogeneities must be viewed as being created by restrictions on the algorithm generating the fractal object. The pixel

limit is, however, more complex and must be considered as an inadequacy of the lattice representation itself.

The probability of an individual pixel being occupied is controlled by the value assigned to p for that stage of the process (for example, at the critical point $p = p_c$). Further, the number of distinct arrangements of, say, 1, 2, 3 or 4 occupied pixels within a given window depends on the window size (for example, one occupied pixel can be placed in four distinct ways in a 2×2 window or sixteen ways in a 4×4 window). As a result, the value of $N(l_m)$ depends on both l_m and p . For small windows, the constraints on $N(l_m)$ are severe and near the pixel limit, the algorithm used to create a percolation invasion pattern is incapable of maintaining the same density of occupied sites as for larger windows. The point is illustrated for a 2×2 window by the the data presented in table 2. There, we presume that the probability of occupation is 0.6 (i.e. site

Table 2
Pixel limit

Event	Probability		
	0.4		
	0.6		
	Probability	Combinations	Product
	$(0.4)^3$	1	0.0064
	$(0.4)^2 (0.6)$	3	0.576
	$3 (0.4) (0.6)^2$	3	1.296
	$(0.6)^3$	1	0.864
		Total	2.7424

percolation threshold of a large grid) and define a "hit" for the 2×2 window whenever at least one of the 1×1 pixels is occupied. We find that statistically the number of hits or number of times the 2×2 square must be covered is 2.7424. Using eq. (4), comparing the 2×2 to the 1×1 window gives as upper bound [11]

$$D_m = \frac{\ln(2.7424/1)}{\ln(2/1)} \approx 1.46.$$

Close to the pixel limit, this way of creating the percolation pattern mimics the effect of low density pixel scale inhomogeneity; the algorithm appears to "create" inhomogeneities near the pixel limit.

2.3. INDUCED INHOMOGENEITIES

Similarly, a percolation invasion algorithm (see the appendix for an example), in concert with the boundary conditions, can create inhomogeneities at large scale. For example, the requirement that the source line be fully occupied and that the process terminate with occupancy of a pixel on the opposite boundary, i.e. the sink line, creates on average the pattern depicted in fig. 4 (cf. ref. [11]). Clearly, this has large scale structure, and for windows of size L and $L/2$, it appears to have dimension two. (Note, however, that if the pattern of interest is not bounded by the perimeter of the grid but is located in one "corner", with the result that the grid is largely empty, the value of D measured with large windows need not be two – it could be much less than one!)

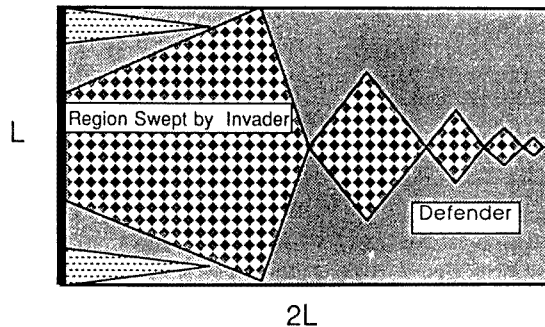


Fig. 4. Schematic of percolation invasion at breakthrough.

In addition, the asymmetry of the source and sink boundary conditions results in large scale lower dimension inhomogeneities near the sink (cf. the large "empty" regions extending back from the sink line in fig. 4). As a result, these inhomogeneities reduce the fractal dimension obtained with windows of size $L/4$, $L/8$, etc. The algorithm appears to create inhomogeneities!

2.4. APPARENT INHOMOGENEITIES

Apparent inhomogeneities are due to deficiencies in the measuring device rather than to inherent deficiencies in the procedure for representing the fractal object or the restrictions of a finite lattice. Perhaps the best example of this is the evaluation of the fractal dimension of a Cantor dust [7].

Table 3
Effect of periodicity

(a) Cantor dust gasket (square)						(b) Sierpinski					
For $l_m = L/3^m$			For $l_m = L/2^m$			For $l_m = L/3^m$			For $l_m = L/2^m$		
m	$N(l)$	D_m	m	$N(l)$	D_m	m	$N(l)$	D_m	m	$N(l)$	D_m
0	1	} 0.63	0	1	} 1	0	1	} 1.893	0	1	} 2
1	2		1	1		1	8		1	4	
2	4		2	4		2	64		2	16	} 2
3	8		3	6		3	512		3	60	
4	16		4	10		4	4096		4	236	} 1.976
5	32		5	16		5	32768		5	864	
6	64		6	28		6			6	3328	} 1.947
			7	42							
									
									
			45	6.308×10^8	} 0.785						
			46	1.087×10^9							
			47	1.638×10^9		} 0.591					

It is well known that if one uses windows (in the Cantor dust, these are simply rulers) which have a periodicity $L, L/3, L/9$, etc., i.e. a periodicity the same as that of the underlying fractal object, then for all window sizes down to the pixel limit one obtains $D_m = 0.63$ (cf. table 3(a)). However, use of rulers of size $L, L/2, L/4$, etc. does not yield a D_m of 0.63. Rather, the oscillating set of values of D_m given in the second column of table 3(a) is obtained; these oscillations are not damped! Thus, the use of rulers with a periodicity different to that of the fractal object appears to generate inhomogeneities at all scales. An analogue in two dimensions is afforded by the Seirpinski gasket using square windows of size $L, L/2, L/4$, etc., rather than the more commonly employed $L, L/3, L/9$, etc. (cf. table 3(b)).

3. Illustration

The representation of the percolation invasion process on a two-dimensional grid will serve to illustrate the application of the issues raised in the preceding section. The fact that the calculated dimension D_m varies with window size is not necessarily a disadvantage for, as pointed out for fig. 2, the resulting structure can provide bounds for D and it can also provide a measure of the scale of the inhomogeneities. This will certainly be the case when the small scale (pixel limit) and large scale inhomogeneities

have a lower dimension than that of the fractal object of interest and there exists only one maximum within this region.

3.1. BOUNDED VALUES OF D_m

To illustrate this point, the values of D_m for the discontinuous defender of an invasion percolation pattern at breakthrough on a two-dimensional square lattice are given in table 4(b); see the appendix for details of the procedure. The curves for D_m are shown in fig. 5 for grid sizes 1024×512 . From this figure, it is clear that the lower

Table 4
Percolation invasion data for a 1024×512 grid

(a) Number of hits (averaged over 300 realizations)									
Window label* m in $l_m = (2)^m$	1	2	3	4	5	6	7	8	9
Continuous invader $N(l_m)$	62517	18618	5214.3	1435.1	393.48	108.01	29.46	7.80	1.96
Discontinuous defender $N(l_m)$	83566	23440	6028.3	1567.0	413.11	110.87	30.07	7.98	2.00
(b) Computed dimension D_m									
Window label* m in eq. (4)	1	2	3	4	5	6	7	8	
Continuous invader D_m (CI)	1.746	1.832	1.858	1.863	1.860	1.871	1.918	1.995	
Discontinuous defender D_m (DD)	1.828	1.953	1.937	1.916	1.891	1.878	1.912	1.995	

*For the 1024×512 grid, the largest $l_m \times l_m$ window is 512×512 , and since $l_m = 2^9 = 512$, the largest window label is $m = 9$ for this grid; the smallest window reported here is 2×2 ($m = 1$), which is one step up from the pixel window of 1×1 .

*For example, the entry 1.918 (at $m = 7$ for D (CI) for the 1025×512 grid is obtained from the data of table 4(a) using eq. (4) as: $D_m = \ln(29.46/7.80)/\ln(2^8/2^7) = 1.329/0.693 = 1.918$.

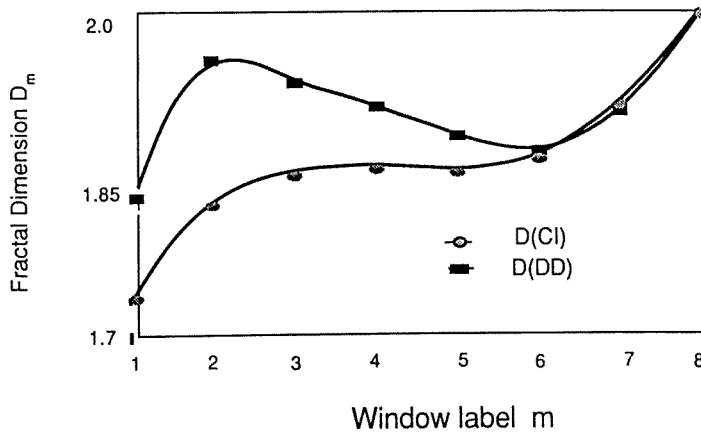


Fig. 5. Fractal dimension versus window label m .

bound of D_m of the discontinuous defender (denoted $D(DD)$) is approximately 1.95, whereas the correct value is $D(DD) = 2.00$, i.e. the discontinuous defender should have the same dimension as the grid. A similar analysis of the continuous invader (CI) yields a lower bound of $D(CI)$ of 1.86. The expected value of $D(CI)$ for invasion percolation when the defending phase is infinitely compressible is 1.896 [5(c), 7, 13] and our lower bound, from fig. 5, implies that $D(CI)$ is at least 1.86.

It is worthwhile noting that the simple average of the $D_m(DD)$ values given in table 4(b) gives unsatisfactory results even if one attempts to remove the effect of the limiting windows. For example, if the smallest and the two largest windows are ignored and the $D_m(DD)$ of table 4(b) are averaged over the remaining windows ($m = 2$ to 6), one obtains values $D_{av}(DD) = 1.91$. Thus, $D_{av}(DD)$ is a less satisfactory result than is obtained by extracting the local maximum. An alternative, and often followed procedure, is to take the number of "hits" $N(l_m)$ for the discontinuous defender given in table 4(a), plot them according to eq. (2) and find the best slope (cf. fig. 1). For the range $m = 2$ to $m = 7$, this gives $D_{fit}(DD) = 1.92$. Thus, the fitting procedure using eq. (2) also yields a less reliable result than is given by the lower bound.

The same points can be made with regard to $D_m(CI)$ values obtained by averaging $D_m(CI)$ values or by fitting $N(l_m)$ versus l_m . The average $D_m(CI)$, obtained from table 4(b) by averaging the $D_m(CI)$ from $m = 2$ to $m = 6$, is $D_{av}(CI) = 1.86$. This average can be "improved" by including the two largest windows, i.e. averaging over $m = 2$ to $m = 8$ to yield $D_{av}(CI) = 1.893$. Although this is very close to correct, the improvement is certainly spurious in that the largest windows are clearly influenced by the boundary (cf. their D_m values of 1.99 and 1.92). The alternative procedure of fitting the $N(l_m)$ given in table 4(a) to eq. (2) gives, for the range $m = 2$ to 7, $D_{fit}(CI) = 1.86$. These values are also often "improved" by including the largest windows, but this must be viewed with suspicion because of the effect of the boundary on the larger windows. Although the case is perhaps not as clear as for $D(DD)$, it is again evident that either averaging $D_m(CI)$ or fitting $N(l_m)$ can give less reliable values of the fractal dimension than the selection of the local maximum in $D_m(CI)$. A knowledge of the inherent structure of the data in table 4 is clearly advantageous!

3.2. EVALUATING THE SCALE OF INHOMOGENEITIES

In the analysis of the preceding paragraphs, the large scale inhomogeneities clearly affect the value of D_m ; indeed, the window size $m = 6$ at which the minimum occurs in fig. 5 indicates that the inhomogeneity spans windows at least as large as $2^6 = 64$, so that inhomogeneities are of order $2^6/2^8 \approx 25\%$ of the entire representation. These large scale inhomogeneities are, of course, a residue of the very asymmetric initial condition of almost 100% defender and only a single source line of invader. On the other hand, the maximum for D_m in fig. 5 between $m = 2$ and $m = 3$ indicates that the small scale inhomogeneity spans windows less than about $2^3 = 8$, so that the inhomogeneity is only $2^3/2^8 \approx 3\%$ of the entire representation.

3.3. PERIODICITY

The only periodicity implied by fig. 5 is that of the limits imposed by the grid extent $L = 1028$ versus the pixel limit $L = 1$. This is, of course, different to the case of the Sierpinski gasket or the Cantor dust discussed previously in section 2.4, where there was an underlying periodicity which was less than that of the grid extent.

3.4. THE INHOMOGENEITY-FREE LIMIT

It is relatively easy to remove the effect of the large scale inhomogeneities by considering only smaller windows. However, as can be seen from fig. 5, the local maximum of D_m , for the discontinuous defender, never reaches its limiting theoretical value of $D(DD) = 2$. This is because the pixel limit encroaches on the windows before they can become small enough to overcome the larger scale inhomogeneities. A larger grid, say 2048×1024 , would provide a greater number of the inhomogeneity-free windows and hence an improved lower bound. An even larger grid would do better, but this is costly if the algorithm generating the fractal is complex. Further, in the case of a physical system, there may be limitations on the measuring device imposed by the extent of the system.

An alternative is to remove the effect of the pixel, thus allowing D_m to approach its proper limit. This is essentially the philosophy of Rapaport, who recognized the possibility of systematic deviations from the asymptotic limit in self-avoiding walks [14] and, of course, many earlier workers had attempted a power series treatment of their data with varying degrees of theoretical motivation (cf. Sykes et al. [15]), McKenzie [16], Middlemiss [17]). One expects the expression for D_m to be a function of the window size l_m associated with each D_m . Since $l_m = 2^m$, one could attempt to fit D_m as:

$$D_m = \sum_i a_i (2^m)^{b_i}.$$

Because of the availability of a high quality statistics routine for fitting a sum of exponentials [18], we have chosen to write

$$D_m = \sum_i \alpha_i e^{\beta m_i}$$

(conversion to a power series in 2^m is effected by the relation $b = 1.44\beta$). On carrying out the procedure, one finds that indeed the fitting function contains a term which is small everywhere except for $m = 1$, i.e. it is the "pixel effect". Fig. 6 displays the curve of D_m versus m for the 1024×512 grid for both the complete fitting function as well as the same function minus the pixel effect. The limit, as $m \Rightarrow 1$, of the corrected curve approaches 1.98 for $D_\infty(DD)$, i.e. it is close to the expected value of 2. For the continuous invader, the corrected curve yields a value of $D_\infty(CI) = 1.89$ as $m \Rightarrow 1$, again

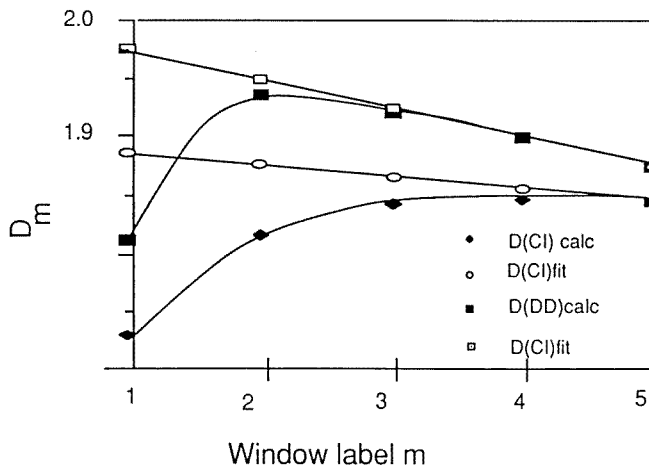


Fig. 6. Correction for pixel effect.

close to the expected value of 1.896. The correspondence of the corrected limiting values of $D_{\infty}(\text{CI})$ and $D_{\infty}(\text{DD})$ to their expected values suggests that this procedure is preferred over either the simple fitting technique for $N(l_m)$ or the averaging procedure for D_m .

We should remark, before leaving this illustration, that the slow convergence of $D_m(\text{CI})$ and $D_m(\text{DD})$ to their correct values is a consequence of inhomogeneities discussed earlier.

4. Concluding remarks

An analysis of the covering properties of adjacent windows with size l_m , where $l_m = 2^m$, $m, m + 1$, yields an expression for the fractal dimension D_m which displays directly effects due to periodicity, boundaries and inhomogeneities. The structure of the D_m versus m curve gives insight into the nature of the representation of the fractal. The size of inhomogeneities can be extracted, as can the periodicity of the underlying structure.

The use of the percolation invasion process at breakthrough provides an elegant example of the role of inhomogeneities. The variation of D_m versus m , illustrated in fig. 2, for a percolation invasion algorithm can be explained in terms of the inhomogeneities shown in figs. 3 and 4. For the largest windows, i.e. $L \times L$, the fractal dimension D_m appears to be two (cf. point C in fig. 1); this is due to the macroscopic structure imposed by the source and sink boundary conditions. However, for a somewhat smaller window, D_m is less than two (cf. point A in fig. 2). This is due to the intrusion (the empty region extending back from the sink, cf. fig. 4) occasioned by the point character of the sink boundary condition which defines the breakthrough condition. Only as the windows become much smaller than these inhomogeneities can the proper value of D assert itself. Eventually, as pixel limit is approached, the value of D_m drops (cf. point

B in fig. 2); this is due to the inability of the algorithm to generate the correct density of occupied pixels.

It is clear that simply fitting D in eq. (2) or averaging over a set of D_m from eq. (4) can yield erroneous values of the fractal dimension [19]. However, an understanding of the dependence of measured values of this dimension on lattice limits, inhomogeneities and periodicity can guide one in extracting the best bounds for D . In some cases, bounds for D may be obtained and, if desired, the effect of the periodicity, of boundaries and of initial conditions can be removed to yield an idealized value of D .

Appendix

Percolation invasion method

The term percolation invasion can refer to a number of processes which ensure that a fluid transport process is represented realistically. Variations of the percolation invasion algorithm depend on details of the step defining breakthrough [20], on whether the trapped fluid is incompressible [21] or infinitely compressible [22], and whether only the single smallest connected site is invaded or whether all connected sites within a size range are invaded [23]. In order to ensure clarity, we outline here, for two dimensions, the algorithm used for the invasion percolation process discussed in the main body of the manuscript.

We consider a square grid of with L and length $2L$ with sites (the grid intersections) labelled $L_{i,j}$, where $1 \leq i \leq L$, $1 \leq j \leq 2L$. The source of the invader fluid is the line of sites $L_{i,1}$ ($1 \leq i \leq L$) and the sink is the line of sites $L_{i,2L}$ ($1 \leq i \leq L$). For a periodic boundary, the edges $L_{1,j}$ and $L_{L,j}$ are neighbours (i.e. as on a cylinder). Sites on the grid are assigned sizes ($0 \leq r \leq 1$) selected at random from a uniform distribution. The initial state has all sites of the source line occupied by the invading phase and all remaining sites occupied by a defending phase, which is taken to be infinitely compressible. Since the invading phase is taken to be wetting relative to a nonwetting defender phase, the invasion process is "imbibition" and is taken to be controlled by the size of the sites.

In the algorithm of the invasion process, we seek the smallest size of defender-occupied site which is contiguous to the invader front (i.e. initially one would test all sites $L_{i,2}$ ($1 \leq i \leq L$) and seek the smallest). Once this single smallest site is identified, it is occupied by the invader. This step creates additional sites contiguous to the invader, and the new set of all sites contiguous to the invader is again examined for the smallest size and when it is found, this single site is invaded; the process is repeated.

In this process, only one site at a time is invaded, each with its own capillary pressure. From a physical point of view, one could imagine carefully controlling the available volume of the invader such that only one site at a time could be penetrated. It should be clear that since sites penetrated are always contiguous to the invader, the algorithm ensures a logical method of transport of material to the site in question. This feature distinguishes between simple percolation and percolation invasion. Further, the use of an infinitely compressible defender fluid removes any need to ensure that the site being penetrated is connected to the sink.

The process terminates when a single site on the sink line is penetrated by the invader – this is "breakthrough".

The result is a two-dimensional pattern of sites occupied by the invader which are, as a consequence of the invasion process, connected to the source – we denote these sites as the continuous invader (CI). The pattern also indicates a number of sites still occupied by the defender but which are totally surrounded (disconnected) by invader-occupied sites – these are denoted as discontinuous defender (DD). Because of the particular termination step chosen, there may be other sites occupied by the defender which are still connected (continuous) to the sink line – they are denoted as continuous defender (CD).

The determination of the fractal dimension requires the evaluation of the number of sites N occupied by a given type of fluid: $N(DD)$, $N(CI)$ and $N(CD)$ denoting, respectively, discontinuous defender, continuous invader and continuous defender. The sum $N(DD) + N(CI) + N(CD) = N(l)$, where $N(l)$ is the number of sites examined in a window of dimension $l \times l$ with $l \leq L$. We confine our examination to square windows $l_m = 2^m$ and when windows of size $l_m \leq L$ are considered, we select them in a regular fashion beginning at one corner of the grid. Each $l_m \times l_m$ window is laid down and, if it contains a site occupied by the type of fluid in question, then a "hit" is registered for that window for that fluid and the sum of hits is recorded as $N(l_m)$. The number of hits for each window size averaged over 300 realizations is given in table 4(a). It is generally agreed that the process just described is equivalent in its static properties to ordinary percolation at breakthrough [24]. Consequently, the continuous invader should have the fractal dimension $D(CI) = 1.896$ or the generally accepted, but unproved, rational value of $91/48$ [13].

Acknowledgements

The support of the National Science and Engineering Research Council of Canada is gratefully acknowledged, as is the support of G.R.H. by the SEED program and of R.M. by the Petroleum Aid to Education Fund. This work received its initial stimulus from the efforts of N.C. Wardlaw and Li Yu to apply their micromodel results for porous media and has benefited from continuing discussions with them. One of the authors (W.G.L.) also acknowledges the stimulus for this work provided by P.P. Crokker and W. Wilson of the Physics Department of the University of Hawaii.

References

- [1] See articles in: *On Growth and Form*, ed. H.E. Stanley and N. Ostrowsky (Nijhoff, Dordrecht, 1986).
- [2] See, for example, recent articles by C. Fairbridge, *Catalysis Lett.* 2(1989)191; P. J. Crickmore and B.S. Larson, *J. Coll. Sci.* (submitted).
- [3] T.A. Witten and L.M. Sander, *Phys. Rev.* B27(1983)5686.
- [4] (a) Li Yu, W.G. Laidlaw and N.C. Wardlaw, *Adv. Coll. Interface Sci.* 26(1986)1; (b) Li Yu and N.C. Wardlaw, *J. Coll. Interface Sci.* 109(1986)461; 473.

- [5] (a) D. Wilkinson and J.F. Willemsen, J. Phys. 16A(1983)3365;
 (b) loc. cit. eq. (2.1) and fig. 1;
 (c) loc. cit. eq. (2.2) and the quoted value of f .
- [6] (a) E. Stanley, J. Stat. Phys. 36(1984)843;
 (b) loc. cit. fig. 5.
- [7] (a) D. Stauffer, *Introduction to Percolation Theory* (Taylor and Francis, London, 1985);
 (b) loc. cit. p. 77, eq. (57);
 (c) loc. cit. p. 52, table 2.
- [8] (a) M. Dias and D. Wilkinson, J. Phys. A (1986);
 (b) loc. cit. eq. (3.3) and fig. 1.
- [9] As pointed out by Farmer et al., D_c may not always be the same as the Hausdorff dimension D_H . Normally, one can take D_c as the better measure of the fractal dimension (see J.D. Farmer, E. Ott and J.A. Yorke, Physica 7D(1983)153).
- [10] R. Orbach, Science 231(1986)773.
- [11] If one calculates analytically the percolation threshold for a 2×2 grid, one obtains $p_c = 0.53$ (and for a 3×3 grid, $p_c = 0.545$). For the 2×2 grid, the average number of sites occupied by the invader is 2.696. Consequently, the number of times one is required to lay down a 1×1 window to cover the object is 2.696, whereas a 2×2 window need only be laid down once to cover this breakthrough pattern. Using eq. (4), this gives $D_0 = [\ln N(l_0/N(l_1))]/[\ln(l_1/l_0)] \approx 1.431$. This will be a lower limit to D obtained for any large grid.
- [12] W.G. Laidlaw, G.R. Hamilton, R.B. Flewelling and W.G. Wilson, J. Stat. Phys. 53(1988)713; see also R. Maier, Ph.D. Thesis, University of Calgary, Calgary, Alberta, Canada T2N 1N4 (1988).
- [13] D. Stauffer, in ref. [1], p. 79; see particularly p. 96.
- [14] D.C. Rapaport, J. Phys. A18(1985)113.
- [15] M.F. Sykes, A.J. Futtmann, A.J. Watts and P.D. Roberts, J. Phys. A5(1972)653;
 M.F. Sykes, D.S. Gaunt and M. Glen, J. Phys. A9(1976)97;
 D.S. Gaunt, M.F. Sykes and H. Ruskin, J. Phys. A9(1976)1899.
- [16] S. McKenzie, J. Phys. A12(1979)L267.
- [17] K.M. Middlemiss, S.G. Whittington and D.S. Gaunt, J. Phys. A13(1980)1835.
- [18] *Biomedical Data Package: Nonlinear Regression* (MBDP Statistical Software Inc., 1964 Westwood Blvd., Los Angeles, CA 90025, USA).
- [19] See R. Meakin, in ref. [1], p. 111; see particularly p. 132, where he remarked that the evaluation of critical exponents is fraught with uncertainty, "more than is usually acknowledged".
- [20] In two dimensions, the disconnection of the defender fluid from the sink and the connection of the source and sink by the invader fluid should, in principle, always occur simultaneously. In finite representations, this does not always occur and the two thresholds can give difference results.
- [21] D. Wilkinson and N. Barsonay, J. Phys. A17(1984)1129; see also ref. [4(a)].
- [22] M.M. Dias and D. Wilkinson, J. Phys. A19(1986)3131, rule 4.
- [23] The authors of ref. [5] comment briefly on this point in paragraph (b).
- [24] H.J. Herrmann, in ref. [1], pp. 3–20.